Materials Today Bio 19 (2023) 100600

Contents lists available at ScienceDirect

Materials Today Bio

journal homepage: www.journals.elsevier.com/materials-today-bio

iPSC-sEVs alleviate microglia senescence to protect against ischemic stroke in aged mice

Xinyu Niu [a,1], Yuguo Xia [c,1], Lei Luo [d], Yu Chen [b], Ji Yuan [b], Juntao Zhang [b], Xianyou Zheng [b,***], Qing Li [b,**], Zhifeng Deng [a,*], Yang Wang [b]

[a] Department of Neurosurgery, Shanghai Sixth People's Hospital Affiliated to Shanghai Jiao Tong University School of Medicine, Shanghai 200233, China
[b] The Institute of Microsurgery on Extremities, Department of Orthopedic Surgery, Shanghai Sixth People's Hospital Affiliated to Shanghai Jiao Tong University School of Medicine, Shanghai 200233, China
[c] Department of Neurosurgery; National Clinical Research Center for Geriatric Disorders, Xiangya Hospital, Central South University, Changsha, Hunan, 410008, China
[d] School of Biomedical Engineering, Shanghai Jiao Tong University, 1954, Huashan Road, Shanghai 200030, China

ARTICLE INFO

Keywords:
Induced pluripotent stem cell-derived small extracellular vesicles (iPSC-sEVs)
Senescent microglia
Ischemic stroke
Aging

ABSTRACT

The polarization of microglia plays an important role in the outcome of ischemic stroke (IS). In the aged population, senescent microglia show a predominant pro-inflammatory phenotype, which leads to worse outcomes in aged ischemic stroke compared to young ischemic stroke. Recent research demonstrated that inducible pluripotent stem cell-derived small extracellular vesicles (iPSC-sEVs) possess the significant anti-ageing ability. We hypothesized that iPSC-sEVs could alleviate microglia senescence to regulate microglia polarization in aged ischemic stroke. In this study, we showed that treatment with iPSC-sEVs significantly alleviated microglia senescence as indicated by the decreased senescence-associated proteins including P16, P21, P53, and γ-H2AX as well as the activity of SA-β-gal, and inhibited pro-inflammatory activation of microglia both *in vivo* and in vitro. Furthermore, iPSC-sEVs shifted microglia from pro-inflammatory phenotype to anti-inflammatory phenotype, which reduced the apoptosis of neurons, and improved the outcome of aged stroke mice. Mechanism studies showed that iPSC-sEVs reversed the loss of Rictor and downstream p-AKT (s473) in senescent microglia, which was involved in the senescence and pro-inflammatory phenotype regulation of microglia. Inhibition of Rictor abolished the iPSC-sEVs-afforded phosphorylation of AKT and alleviation of inflammation of senescent microglia. Proteomics results indicated that iPSC-sEVs carried transforming growth factor-β1 (TGF-β1) to upregulate Rictor and p-AKT in senescent microglia, which could be hindered by blocking TGF-β1. Taken together, our work demonstrates iPSC-sEVs reverse the senescent characteristic of microglia in aged brains and therefore improve the outcome after stroke, at least, via delivering TGF-β1 to upregulate Rictor and p-AKT. Our data suggest that iPSC-sEVs might be a novelty therapeutic method for aged ischemic stroke and other diseases involving senescent microglia.

1. Introduction

Stroke is the second leading cause of death worldwide [1], and ischemic stroke accounts for over 80% of stroke patients [2]. Stroke-induced robust inflammation aggravates the second brain injury by enhancing excitotoxicity, oxidative stress, and direct cytolysis [3]. It is demonstrated that the intensity of inflammation response is correlated with the severity of brain damage and long-term outcomes in stroke patients [4]. Thus, regulation of post-stroke inflammation has been a prime target for the treatment of ischemic stroke [5].

* Corresponding author. Department of Neurosurgery Shanghai Sixth People's Hospital Affiliated to Shanghai Jiao Tong University School of Medicine 600 Yishan Road, Shanghai 200233, China
** Corresponding author. Institute of Microsurgery on Extremities, Department of Orthopedic Surgery Shanghai Sixth People's Hospital Affiliated to Shanghai Jiao Tong University School of Medicine 600 Yishan Road, Shanghai 200233, China
*** Corresponding author. Institute of Microsurgery on Extremities, Department of Orthopedic Surgery Shanghai Sixth People's Hospital Affiliated to Shanghai Jiao Tong University School of Medicine 600 Yishan Road, Shanghai 200233, China
E-mail addresses: zhengxianyou@126.com (X. Zheng), liqing_236@aliyun.com (Q. Li), zfdeng@sjtu.edu.cn (Z. Deng).
[1] Xinyu Niu and Yuguo Xia contributed equally.

https://doi.org/10.1016/j.mtbio.2023.100600
Received 27 November 2022; Received in revised form 27 February 2023; Accepted 1 March 2023
Available online 4 March 2023

Microglia, the innate immune cell in the central nervous system (CNS), are the first responders to ischemic stroke and play a crucial role in post-stroke neuroinflammation [6]. When stimulated by pathological stress, such as ischemic injury, the "resting" microglia are activated and adopt different functional phenotypes. M1-like pro-inflammation microglia aggravate brain injury by secreting multiple proinflammatory factors, such as tumor necrosis factor-α (TNF-α) 、interleukin-6 (IL-6)、interleukin-1β (IL-1β) [7,8], which exert neurotoxic effect on neuron and increase the death of neuron in ischemic stroke [9]; M2-like anti-inflammation microglia exert protective effect by producing anti-inflammatory cytokines containing transforming growth factor-β (TGF-β)、interleukin-10 (IL-10), and neurotrophic factors [8]. Recent researches indicate that microglia displayed senescent phenotype in both aged mice and human brain [10–12]. Senescent microglia become activated and tend to be pro-inflammation phenotype, which leads to worse neurological function in aged stroke mice compared to young stroke mice [13,14]. Therefore, we predict that alleviating the senescence of microglia could improve the outcome of ischemic stroke in aged mice.

Stem cell derived small extracellular vesicles (sEVs), the lipid bilayer nanovesicles, possess the similar capacity to their parental cell and exert function by delivering encapsulated cargo such as proteins, nucleic acids to recipient cells. In our previous studies, embryonic stem cells (ESCs) derived sEVs alleviate senescence of bone marrow-derived mesenchymal stem cells (BM-MSCs) and prevent age-related bone loss [15]. Systematic administration of ESC-sEVs can also rejuvenate senescence of hippocampal neural stem cells (NSCs) and improve cognitive deficiency during natural aging [16] and in a rat model of vascular dementia (VD) [17]. Induced pluripotent stem cells (iPSCs) are another kind of pluripotent stem cells (PSCs) with unlimited self-renewal and differentiation capacity similar to ESC [18]. iPSCs can be generated specifically from patients' biopsies, and avoid ethic issues and immune-rejection [19,20], therefore is a promising seed cells for regenerative medicine. Recent research indicated iPSC-sEVs could alleviate senescence of MSCs [18]. Whether iPSC-sEVs could alleviate microglia senescence and regulate senescent microglia-induced inflammation in aged ischemic stroke has not been investigated.

Herein, we first investigated the rejuvenating ability of iPSC-sEVs on senescent microglia, and then evaluated the capacity of iPSC-sEVs to alleviate senescent microglia-induced neuroinflammation and neurological deficits after ischemic stroke in aged mice. We found that iPSC-sEVs alleviated senescent phenotype of microglia *in vitro* in the D-gal-induced cell senescence model and *in vivo* in normal aging mice, and therefore inhibited senescent microglia-induced inflammation. Besides, iPSC-sEVs regulated polarization of microglia from pro-inflammatory phenotype to anti-inflammatory phenotype in aged stroke mice, which led to reduced neuronal death and improved neurofunctional recovery. We further showed that the regulatory function of iPSC-sEVs on microglia was, at least, through delivering TGF-β1 to promote the expression of Rictor and phosphorylation of AKT. Our study proved the therapeutic effect of iPSC-sEVs against ischemic stroke in the elderly via inhibiting microglia senescence and the related neuroinflammation, which provides a potential alternative for aged ischemic stroke and other aging-related neuroinflammatory diseases in the central nervous system (CNS).

2. Methods

2.1. Culture and identification of iPSCs

We have been approved to use human iPSC in this study by the local ethics committee of the Shanghai Sixth People's Hospital affiliated with Shanghai Jiao Tong University. The human iPSC line nciPS01 (RC01001-A, male, Nuwacell Biotechnology CO., Ltd) was provided by Nuwacell Biotechnology. The details of iPSCs culturing were as previously described [21]. Briefly, a six-well plate coated with vitronectin human recombinant protein (RP01002, Nuwacell Biotechnology CO., Ltd) and ncEpic hPSC medium (RP01001, Nuwacell Biotechnology CO., Ltd) were prepared, then iPSCs were seeded and cultured in it. The supernatant was collected for subsequent experiment and the cells were sub-cultured when reaching 90% confluence. iPSCs colonies expressing pluripotency-related markers (Nanog, OCT4, SSEA4, TRA-1-60, TRA-1-81) were identified by immunofluorescence staining.

2.2. Culture of BV-2 cells

Mouse microglia cell lines BV2 were purchased from Central for Cell Resources of Chinese Academy of Medicine Sciences. BV2 cells were cultured in complete medium containing high glucose DMEM (Corning) and 10% fetal bovine serum (FBS, Gibco) at 37 °C with 5% CO_2. The cells were passaged when the confluency reached to 80–90%.

2.3. Culture of fibroblast cells

Human fibroblast cell line (HFF-1) was obtained from National Collection of Authenticated Cell Cultures. The fibroblast cells were cultured in complete medium containing high glucose DMEM (Corning) with 10% fetal bovine serum (FBS, Gibco) and 1% glutamax (Gibco) at 37 °C with 5% CO_2. When the confluency reached to 80%, the cells were passaged.

2.4. Derivation and culture of iPSC-derived MSCs

The human induced pluripotent stem cell line (iPS-S-01) was obtained from the Institute of Biochemistry and Cell Biology of the Chinese Academy of Sciences in agreement with Liao and Xiao [22]. hiPSC-MSCs (iMSC) were generated as our previous report [23]. iMSCs were cultured in the serum-free hMSC medium (RP02010, Nuwacell Biotechnologies, China). When the confluency reached to 80%, the cells were passaged.

2.5. Isolation of iPSCs-sEVs

iPSC-sEVs were isolated and purified from the above collected supernatant by classical differential centrifugation/ultracentrifugation method according to the 2018 guideline [24]. Briefly, the supernatant was centrifuged at 300×*g* for 10 min, 2000×*g* for 10 min, and 10,000×*g* for 1 h to remove cells, dead cells, cell debris, and microvesicles (MV). Then, the supernatant was collected to ultracentrifuge at 10,0000×*g* for 70 min twice. After removing the supernatant, the small extracellular vesicles (sEVs) were resuspended in sterile PBS.

2.6. Identification of iPSCs-sEVs

2.6.1. Size distribution and concentration

We used a high-resolution nanoflow cytometer to assess particle diamater and particle concentration of iPSCs-sEVs as previously described [25]. First, for the measurement of particle concentration, standard polystyrene nanoparticles (diameter: 200 nm; concentration: 1.58×10^8/ml) were used to measure side scatter intensity (SSI), then the SSI of the iPSCs-sEVs were evaluated and particle concentration were calculated by the SSI. For the measurement of particle size, four standard silica nanoparticles with different sizes (diameter: 68, 91, 113, 155 nm) were used to generate stand curve, and the size distribution was calculated accordingly.

2.6.2. Transmission electron microscope (TEM)

Firstly, iPSCs-sEVs were dried on the formvar-carbon-coated grid at room temperature for 20 min and then were fixed in 1% glutaraldehyde. Next, sEVs were washed by dd water and stained with saturated aqueous uranyl oxalate for 5 min. Finally, the morphological images of sEVs were captured by TEM.

2.6.3. Western blot analysis of iPSCs-sEVs

iPSCs-sEVs were washed twice with phosphate buffer saline (PBS) by ultracentrifugation. Then we added RIPA lysis buffer (P0013C, Beyotime Biotechnology) to the sEVs pellet, and protein concentration was measured by BCA kit (P0012S, Beyotime Biotechnology). Finally, western blot experiment was performed as following described. Briefly, electrophoresis, membrane transfer followed by incubation of primary antibodies, including anti-CD9 (Abcam, ab92726), anti-TSG-101 (Santa cruz, sc-7964), anti-CD63 (Abcam, ab134045), anti-Lamin A/C (Servicebio, GB11407), and anti-GM130 (Abcam, ab52649). After incubation overnight, secondary antibodies were added to the membrane and proteins bands were exposed by the ChemiDoc™MP Gel Imaging System (Bio-rad).

2.7. Animals and MCAO procedure

All animal procedures were approved by the Animal Research Committee from Shanghai Sixth People's Hospital (SYXK [Shanghai, China] 2011–0128, 1 January 2011). Male C57/BL6 mice (age: 2 months or 16 months; weight: 25–30 g) were cared at the animal facility and used for the following experiment in Shanghai Sixth People's Hospital. All aged mice were randomly separated to different two group by using the lottery box and the MCAO procedure was performed by another assistant who was blinded to the grouping design. Next, a transient middle cerebral artery occlusion (MCAO) method used to mimic ischemic stroke was performed in mice as previously described [26]. Briefly, mice were anesthetized using 5% isoflurane and then were gently placed on the operating table. A silicon suture (Doccol) was inserted in the middle cerebral artery (MCA) to block blood flow for 60 min. After the operation, mice were placed to their home cage and carefully cared. During the MCAO procedure, regional cerebral blood flow (rCBF) was measured. The mortality rate in Young + PBS + MCAO group, Aged + PBS + MCAO group and Aged + sEVs + MCAO group was approximately 10%, 16% and 13%, respectively. The mice who died after the MCAO or whose rCBF reduced less than 50% after suture insertion were excluded.

2.8. Measurement of regional cerebral blood flow

The rCBF reflected the blood flow of middle cerebral artery and a laser Doppler flowmetry (moorFLPI-2) was used to detect the change of rCBF before, during and after MCAO. The rCBF dropped 70% or increased 50% compared to the pre-MCAO level when the suture was inserted or removed, which indicated the MCAO model was successful.

2.9. iPSC-sEVs administration

iPSC-sEVs (10^9 particles in 200 μL PBS) or PBS (200 μL) were pre-administrated to mice once a week for 2 months (from 16 months to 18 months) in “aged group”. PBS (200 μL) was pre-administrated to mice as a same frequency for 2 months in “young group”.

2.10. Immunofluorescence staining

For the preparation of brain tissues, mice were sacrificed and then perfused with cold normal saline (NS). Brain samples were harvested and immersed in 4% PFA for 1 day and then transferred to gradient sucrose solutions (20%, 30%, 35%) for dehydration at 4 °C. Next, the brain samples were embedded with OCT (optimal cutting temperature compound) and frozen in −80 °C freezer. The embedded brain samples were cut into sections (25 μm thick) by freezing microtome (Leica CM 1950; Leica Biosystem) for following staining experiment. For the preparation of cell samples, the medium was removed and cells were washed with PBS three times. In the staining step, samples were permeabilized with Triton-X-100 (SOLARBIO, CAT# T8200), and then washed with PBS three times. Next, samples were blocked with 5% bovine serum albumin (BSA, Sigma) and incubated with following different primary antibodies against IBA1 (Abcam, ab178847), IBA1 (Snta Cruz Biotechnology, sc-32725), Rictor (proteintech, 27248-1-AP), p-AKT (CST, 4060), P16 (Abcam, ab189034), γ-H2AX (Cell Signaling Technology, CST, 9718s), MAP-2 (CST, 4542s), CD16/32 (BD Biosciences, 553,142), CD206 (R&D Systems, AF2535) and NeuN (CST, 24,307). Then, secondary antibodies (Invitrogen) were added and nucleus were stained with DAPI (Sigma). For TUNEL staining, samples were stained according with manufacturer's instructions (Beyotime biotechnology, C1089). The pictures were captured by fluorescence microscope (DM6B or DM8, Leica).

2.11. Western blot

For western blot analysis of BV2 cells, the cells were washed three times using cold PBS and collected in tube. RIPA solution (EpiZyme) was added to tube to obtain protein solution. Protein concentration was measured by BCA Protein Assay Kit (Beyotime) as manufacturer's instructions. Equal amounts of proteins were separated by SDS-PAGE and transferred to a PVDF membrane. Then the membrane was blocked with 5% milk for 1 h at room temperature (RT) and incubated with primary antibodies against P16 (Invitrogen, MA5-17142), P21 (Abcam, 109,199), P53 (CST, 2524), γ-H2AX (CST, 9718s), β-Tubulin (Affinity, AF7011), β-actin (Abcam, 179,467), Akt (CST, 9272), p-AKT (CST, 4060) and Rictor (proteintech, 27248-1-AP) at 4 °C overnight. After that, HRP-linked anti-IgG secondary antibodies were applied and proteins bands were visualized using WB imaging instrument (FluorChem M, ProteinSimple, Santa Clara, CA, USA).

2.12. Cresyl violet (CV) staining

Firstly, brain sections were dehydrated in gradient ethanol (75%, 85%, 95% and 100%), followed by a rehydration process in another gradient ethanol (100%, 95%, 85%, 75%, 50%). Then the brain sections were stained with CV solution (C5042, Sigma-Aldrich) at 37 °C for 15 min. Next, a decolorization process was performed and then brain sections were immersed into xylene twice for 5 min per time. At last, the brain slides were mounted with neutral resins.

2.13. Analysis of morphology and number of microglia

Three 15 μm-thick brain sections at every 200 μm interval were used for immunohistochemical staining to detect $Iba1^+$ microglia. Two random fields of every sections within grey matter and white matter were chosen for the next analysis and each group contained four mice. Mean length of process, mean volume of soma, and the total number of microglia was analyzed by Image J. The design of grouping was blinded to operator.

2.14. Measurement of infarct volume

The infarct volume after 3 days MCAO procedure was evaluated. Firstly, brain selections were stained by MAP-2 or cresyl violet, two different manners to label brain tissues. The infarct volume was calculated by summing the infarct area of each section (the total volume of contralateral side minus the uninjured total volume of ipsilateral side). The infarct ratio was that infarct volume/healthy volume × 100%.

2.15. Total RNA extraction and real-time quantitative PCR (RT-qPCR)

For brain tissues RNA extraction, mice were sacrificed and then perfused with cold NS. The ipsilateral infarct brain was dissected and homogenized with lysis buffer (EZBioscience), and total RNA was extracted using Tissue RNA Purification Kit Plus (EZBioscience). The RNA of BV2 cells was extracted using Cell/Tissue Total RNA Isolation Kit V2 (Vazyme) as instructions. The reverse transcription response was performed using Color Reverse Transcription Kit (EZBioscience). Then the RT-qPCR was carried out on an ABI Prism 7900HT real-time system

(Applied Biosystems) and the related primer information was shown in supplemental table. The data was calculated according to $2^{-\Delta\Delta Ct}$ approach to obtain the relative mRNA expression of different genes.

2.16. Neurological score (NS)

Neurological score was assessed starting from 2 h (0 day) to 3 days after MCAO operation once a day. The details were as following: "0 point", normal or without obvious neurological deficits; "1 point", could not extend right forepaw completely; "2 point", circle to right; "3 point", could not stand up and fell to the right side; "4 point", no spontaneous movement; "5 point", no response to exogenous stimulation or death.

2.17. Behavior tests

The behavior tests containing rotarod test, adhesive test and cylinder test were used to assess neurological deficits up to7 days post MCAO procedure. In order to decrease errors, mice were trained for 5 days before operation. The rotarod test was used to evaluate the locomotor function. Briefly, mice were forced to run on a rotating drum with the accelerating speed from 5 to 40 rpm within 4 min as fast speed and from 5 to 20 rpm within 5 min as slow speed. The mean time mice stayed on the drum was defined the latency to fall [27]. The adhesive test was used to evaluate the tactile response and sensorimotor function [26]. A sticker with 3 mm in width and 3 mm in length was pasted onto the right paralyzed forepaw, then the mouse was put back to cage and we began to count the time. The touch time was defined as the time mouse started to bit the sticker and the remove time was defined as the time mouse successfully tear off the sticker. The cylinder test was utilized to evaluated forepaw use and rotation asymmetry [28]. Briefly, mouse was placed in a 15-cm-height and 9-cm-diameter cylinder, then we used camera to record the number that mouse contacted the wall by its forepaws (left, L; right, R; both, B). The asymmetric rate was calculated as (L-R)/(L + R + B) × 100 (%).

2.18. Induction of BV2 senescence by D-galactose

We used D-gal, a chemical method [17,29], to induce BV2 senescence. Briefly, 20 g/L sterile D-gal was diluted in complete medium containing high-glucose DMEM and 10% FBS. The cells cultured in medium containing D-gal with PBS or iPSC-sEVs (1×10^9 particles/ml) were consecutively sub-cultured for 8 passages until the senescence phenotype was presented by BV2. In some experiments involving inhibitors, 0.5 μm PP242 (MedChem Express) or 10 μm SB525334 (Selleck Chemicals) was added to the medium from passage 2 to passage 8 to inhibit the biological function of Rictor or TGF-β1 respectively. The cells in control group were cultured in medium with same volume PBS but without D-gal and iPSC-sEVs, and sub-cultured in same passages. Control + PBS group referred to young microglia; D-gal + PBS group referred to senescent microglia; D-gal + sEVs group referred to rejuvenated senescent microglia.

2.19. Detection of distribution of iPSC-sEVs in vivo

sEVs (diluted in 200 μL PBS) were labelled with PKH26 dye (4 mM, Sigma) for 10 min at room temperature and ultracentrifugation process (100,000 g for 114 min) was performed to exclude the un-labelled dye. Then the sEVs were administrated through the tail vein to mice. After 24 h, the mice were anesthetized, and then the distribution of iPSC-sEVs in various organs were recorded by the IVIS Spectrum system (Perkin-Elmer, USA).

2.20. BBB crossing model

Mouse brain endothelia cells line (b End.3 cells) were purchased from Cell Bank, Chinese Academy of Sciences and were cultured in high-glucose DMEM containing 10% FBS. The in vitro BBB model was established according to previous methods [30–33]. Briefly, 1×10^5 b End.3 cells were seeded in the upper chamber of transwell with 0.4 μm-bore diameter (Corning 3640) and BV2 cells were seeded in the lower plate of the transwell. The cells were cultured for 2 days until b End.3 cells reached 100% confluency to form tight junctions, and then the same DiI-labelled iPSC-sEVs were added to the upper insert to detect the BBB-crossing ability of iPSC-sEVs. After 6 h, BV2 cells were stained by DAPI, and images were captured by DM8 (Leica).

2.21. Uptake of iPSC-sEVs in vivo and in vitro

For the detection of iPSC-sEVs *in vivo*, sEVs (2×10^9 particles) were labelled with Dil dye (10 μM, Thermo Fisher) for 30 min at 37 °C, and then we performed the ultracentrifugation process (100,000 g for 114 min) to exclude the un-labelled dye. Then the sEVs (diluted in 200 μL PBS) were administrated through the tail vein to mice. After 24 h, the mice were sacrificed and brain selections were prepared as above mentioned. Next, microglia were stained with Iba1 and nucleus was stained with DAPI (Sigma). For the detection of uptake of sEVs in vitro, Dil-labelled sEVs were added to medium of BV2, and then cells were fixed and stained with Actin-FITC (Beyotime, C1033) and DAPI. The images of uptake were captured with DM6 microscope.

2.22. Evaluation of activity of senescence-associated beta-galactosidase (SA-β-gal)

We used the Senescence β-Galactosidase Staining Kit (Beyotime) to detect the activity of SA-β-Gal as manufacturer's instructions. Briefly, BV2 cells were fixed for half hour and then washed with PBS three times. Next, the staining reagent was added to the cells for 24 h at 37 °C. Images were captured by DM6 microscope and data were analyzed by Image J.

2.23. Oxygen and glucose deprivation (OGD) model

We used the OGD model to mimic ischemic stroke in vitro. Briefly, we replaced the previous complete medium of BV2 with DMEM without glucose and FBS. Then cells were transferred to an incubator (PH-A001) with 95% N_2, 5 CO_2, and 0.1% O_2 supply for 2 h. Next, the cells were cultured in normal medium containing DMEM (Corning) and 10% FBS (Gibco) for 24 h to imitate reperfusion process after MCAO.

2.24. Coculture Sh-sy5y and different age state of microglia

Firstly, different age state of microglia (young microglia referred to BV2 treated with PBS but without D-gal and iPSC-sEVs; senescent microglia referred to BV2 treated with D-gal and PBS; rejuvenated microglia referred ro BV2 treated with D-gal and iPSC-sEVs) were seeded upper small chamber and neuron cell line-Sh-sy5y cells were seeded in under hole plate. The transwell with the 0.4 μm-bore diameter (Corning 3640) only allowed cytokines but not cell to penetrate. After cells adhered the plate, we replaced the previous complete medium of BV2 and Sh-sy5y with DMEM without glucose and FBS. Then co-cultured system were transferred to an incubator (PH-A001) with 95% N_2, 5 CO_2, and 0.1% O_2 supply for 2 h. Last, the medium in both upper small chamber and under hole plate of the transwell was returned to normal medium containing DMEM (Corning) and 10% FBS (Gibco) for 24 h to imitate reperfusion process after MCAO.

2.25. Flow cytometry analysis

Firstly, the BV2 cells were collected and washed with PBS containing 1% FBS twice. Then, 1×10^6 cells were stained with fluorophore-labelled antibody: CD86-PE (BD Pharmingen, 561,963, 1/100) or Isotype control-PE (Rat IgG2α, BD Pharmingen, 557,229, 1/100). For the detection of CD206-positive cells, BV2 cells were permeabilized and fixed with

intracellular staining kit (eBioscience) and then labelled with CD206-Alexa Fluor®647 (BD Bioscience, 565,250, 1/100) or Isotype control-Alexa Fluor®647 (Rat IgG2α, BD Bioscience, 557,690, 1/100). Next, data were obtained in FACSCanto II flow cytometer and processed by FlowJo software (v10.6.2).

2.26. Statistical analysis

All the data were analyzed by GraphPad Prism (version 8.2.1) and presented as the mean ± SD. one-way ANOVA was used for difference among three or more groups. The two-way repeated ANOVA was employed for differences in means across three or more groups over time. Tukey test or Bonferroni test was used for *post hoc* test for equal SDs. Dunnett's T3 was used for *post hoc* test when we did not assume equal SDs.

3. Results

3.1. Characteristics of iPSCs and iPSCs-sEVs

iPSCs colonies expressed the representative pluripotency-related markers, including Nanog, OCT4, SSEA4, TRA-1-60 and TRA-1-81 (Fig. 1A). Then we isolated iPSCs-sEVs from the collected supernatant of iPSCs by ultracentrifugation. The purified iPSCs-sEVs displayed particle size ranging from 30 to 150 nm with diameter of 81.14 nm ± 17.35 nm (Fig. 1B). Western blot analysis showed that iPSC-sEVs positively expressed exosomal markers (CD9, CD63, and TSG101) and were negative for Lamin A/C and GM130 (Fig. 1C). iPSCs-sEVs showed the typical cup-shaped morphology under TEM (Fig. 1D).

3.2. iPSC-sEVs alleviated microglia senescence and restrained pro-inflammation phenotype polarization in vitro

To investigated whether iPSC-sEVs could rejuvenate senescent microglia, we first induced BV2 (a mouse microglia cell line) cell senescence in vitro by treatment with D-gal, a chemical method used to induce cell senescence as previously described [17,29]. Then, we assessed the anti-senescence effect of iPSC-sEVs on microglia. Dil-labelled iPSC-sEVs could be successfully taken up by BV2 cells (Fig. S1). To verify that iPSC-sEVs could cross BBB to be taken by microglia, we used transwell to construct an in vitro BBB model (Fig. S2A). The same particles of DiI-labelled sEVs were added to the medium in the insert and BBB model did not significantly influence uptake efficiency of microglia (Fig. S2B) after the same incubation time. The above results indicated sEVs could cross BBB to be taken by microglia. The western blot result showed that senescence-related proteins (P16, P21, P53) [16,29] and DNA damage marker γ-H2AX [16,17] were significantly upregulated in D-gal-treated BV2 cells, while iPSC-sEVs

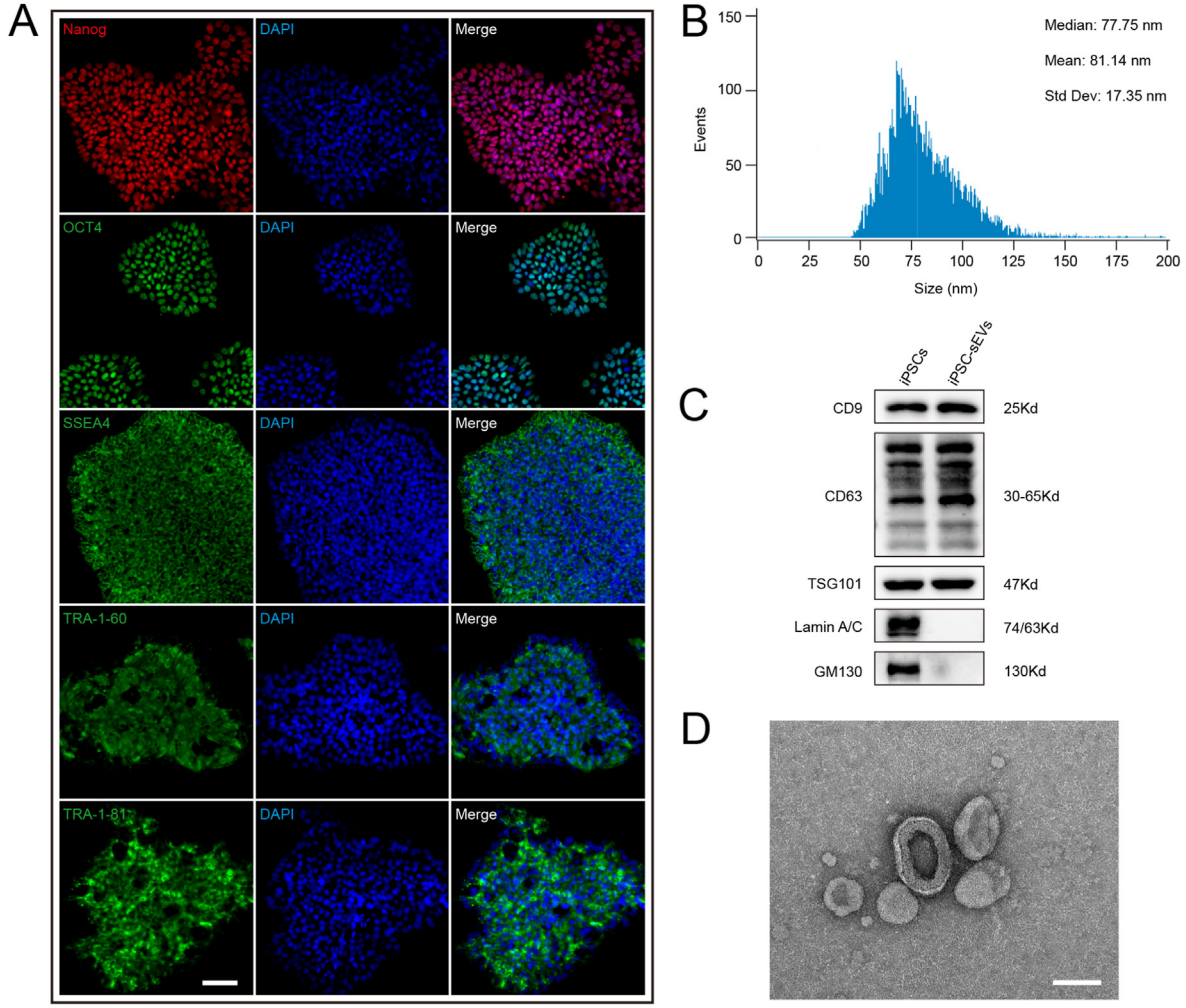

Fig. 1. Characteristics of iPSCs and iPSC-sEVs. (A) Representative fluorescent images of Nanog, OCT4, SSEA4, TRA-1-60, TRA-1-81 and DAPI. Scale bar: 50 μm. **(B)** Particles diameter distribution of iPSCs-sEVs identified by nanoflow cyometer. **(C)** Identification of iPSCs-sEVs by western blot showed the positive markers (CD9, CD63, TSG101) and negative for (Lamin A/C, GM130). **(D)** Representative morphological image of iPSCs-sEVs captured by TEM. Scale bar: 100 μm.

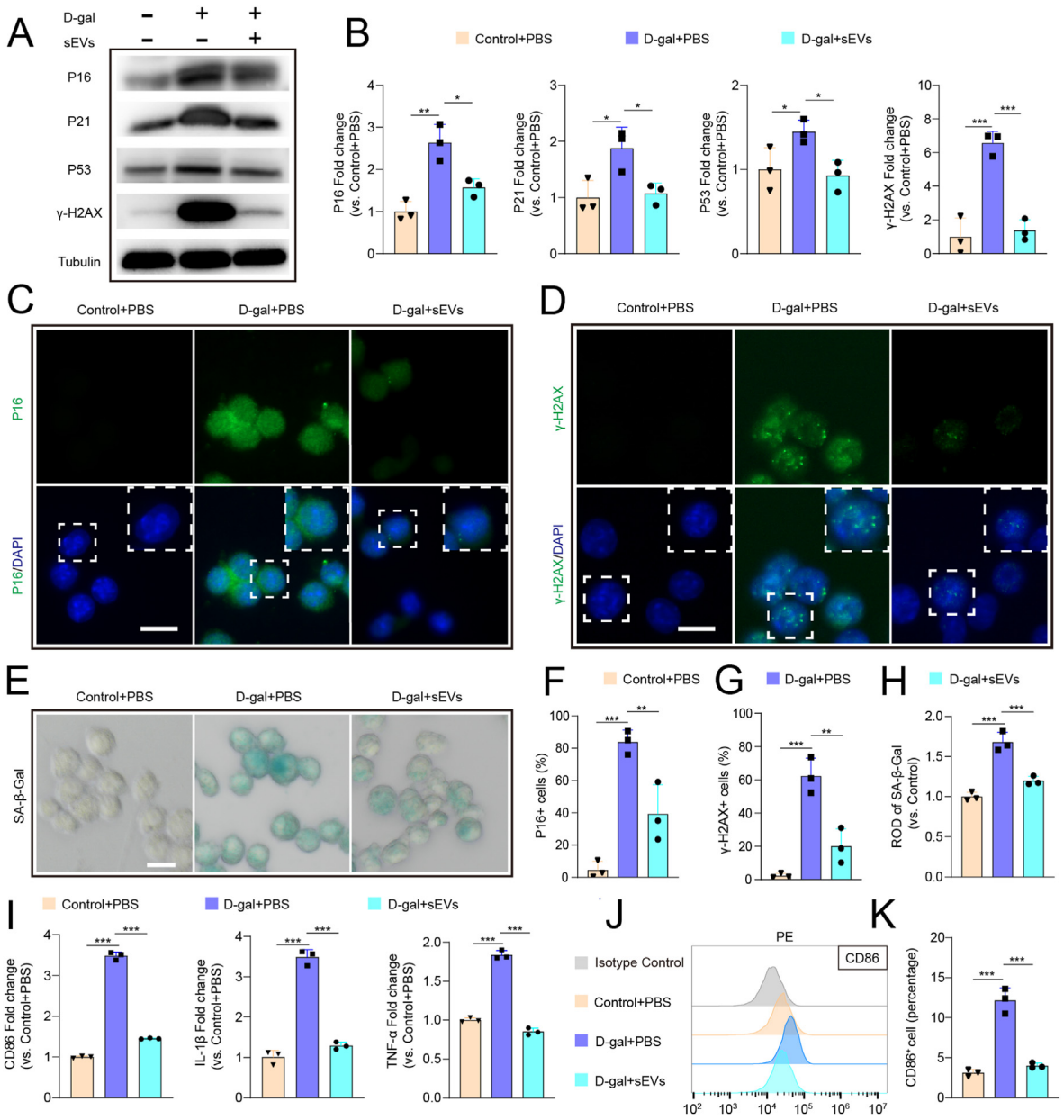

Fig. 2. iPSC-sEVs alleviated D-gal induced senescence and senescence-related pro-inflammatory activation of microglia. (A–B) Represent western blot bands **(A)** and quantification **(B)** of senescence-related proteins: P16, P21, P53, γ-H2AX in BV2 cells. n = 3 per group. **(C–D)** IF staining images of P16 **(C)** and γ-H2AX **(D)**. Scale bar: 25 μm. **(E)** SA-β-Gal images of BV2. Scale bar: 25 μm. **(F–H)** Quantification of positive percentage of P16 **(F)**, γ-H2AX **(G)** relative to total cells, and quantification of activity of SA-β-Gal **(H)** relative to control + PBS group. n = 3 per group. **(I)** Quantification of RNA level of M1-microglia markers (CD86, IL-1β, TNF-α) relative to control + PBS group. **(J)** Flow cytometry histogram of $CD86^+$ BV2 cells. **(K)** Quantification of percentage of $CD86^+$ cells. n = 3 per group. Statistical significance was calculated by one-way ANOVA. *P < 0.05, **P < 0.01, ***P < 0.001.

reversed the increased expression of these proteins (Fig. 2A–B). Immunofluorescence (IF) staining results showed that incubation with iPSC-sEVs also attenuated D-gal-induced increase of $P16^+$ cells (Fig. 2C and F) and γ-$H2AX^+$ cells (Fig. 2D and G) number in BV2 cells. Additionally, the increased activity of senescence-associated beta-galactosidase (SA-β-Gal), another marker for senescence [16] induced by D-gal, was ameliorated by addition of iPSC-sEVs (Fig. 2E and H). These results indicated that iPSC-sEVs could rejuvenate D-gal-induced senescence in microglia. Besides, we also explored anti-senescence effect of sEVs derived from fibroblast cells, usually used to reprogram to produce iPSC [34], and sEVs secreted by iPSC-derived MSC (iMSC) on microglia. It was interesting that fibroblast-sEVs had little effect on the expression of senescence-related proteins, and iMSC-sEVs only reduced the expression of γ-H2AX compared to D-gal + PBS group (Figs. S3A–B). The above results indicated that the anti-senescence ability of iPSC-sEVs reported in this work was not general for other types of sEVs including fibroblast-sEVs and iMSC-sEVs. It is reported that senescent microglia are activated and polarized toward the pro-inflammation type with upregulated expression of markers of M1-like microglia and inflammatory factors [12,35]. Therefore, we further evaluated microglia-related pro-inflammatory genes (CD86, IL-1β, and TNF-α) by qPCR. We found addition of D-gal upregulated the expressional level of CD86, IL-1β and TNF-α as expected (Fig. 2I); Incubation with iPSCs-sEVs reversed the above changes (Fig. 2I). Furthermore, flow cytometry results indicated that the percentage of $CD86^+$ cells was higher in D-gal + PBS group compared to control + PBS group, treatment with iPSCs-sEVs decreased

the D-gal-induced high expression of CD86 (Fig. 2J–K). Taken together, these results indicated that iPSC-sEVs alleviated the microglia senescence, therefore restrained pro-inflammatory phenotype polarization of senescent microglia in vitro.

3.3. iPSC-sEVs alleviate microglia senescence and ageing-associated neuroinflammation in aged brain

In order to verified whether iPSC-sEVs could alleviate microglia senescence in aged mice. We firstly determined distribution of iPSC-sEVs *in vivo*. PKH26-labelled iPSC-sEVs was injected to the mouse by tail vein, and 24 h later the fluorescence was focused in brain and abdomen in the whole mouse image (Fig. S4A). Next, by dissecting organs, we showed that the fluorescent signal was mainly in liver, spleen, intestine (Fig. S4B), while there was also partial signal detected in brain (Fig. S4C), indicating that iPSC-sEVs could be successfully delivered to brain. Moreover, DiI-labelled sEVs were co-stained with $Iba1^+$ microglia, indicating iPSC-sEVs could cross BBB and be up-taken by microglia (Fig. S5). Then, 16-month-old mice were administrated with iPSC-sEVs or PBS for 2 months. IF staining results showed that iPSC-sEVs significantly decreased the percentage of senescent microglia ($Iba1^+P16^+$) (Fig. 3A–B). The morphologic change is another characteristic of senescent microglia. The IHC staining of Iba1 showed that in the aged brain, the process of microglia became less and shorter compared to microglia in young brain (Fig. 3C), which was described as the dystrophic morphology [11,36], while iPSC-sEVs treatment increased the number and length of branches of microglia (Fig. 3C). However, we did not find the difference in the volume of soma and total number of microglia among three groups (Fig. 3C). The process of microglia is an important element in exerting function [37], for example, microglia can sense the damage signal and trigger inflammatory response by their high branched process [38,39]. The correction of dystrophic morphology indirectly indicated that ageing-associated dysregulated function was partly reversed. Senescent microglia are activated and secret pro-inflammatory factors, which is the source of chronic neuroinflammation in aged brain [36]. IF was used to detect the pro-inflammatory microglia ($CD16^+Iba1^+$) in young and aged brain. The results showed that compared to that of the young mice, the percentage of $CD16^+$ microglia significantly increased in aged brain, which was decreased by iPSC-sEVs treatment (Fig. 3D–E). Accordingly, the RNA expression of M1-related pro-inflammatory genes including CD86 (Fig. 3F), IL-1β (Fig. 3G) and TNF-α (Fig. 3H) increased in aged brain, and were attenuated by iPSC-sEVs administration (Fig. 3F–H). These results indicated that iPSC-sEVs could alleviate microglia senescence, inhibit microglia pro-inflammatory activation, and attenuate ageing-associated neuroinflammation in aged brain.

3.4. iPSC-sEVs attenuated inflammatory response of senescent microglia and reduced neuronal apoptosis in aged stroke mice

We further evaluated the protective effect of iPSC-sEVs in aged stroke mice. The stroke model was generated by MCAO in young with PBS and aged with PBS or iPSC-sEVs mice. Firstly, the regional cerebral blood flow (rCBF) of mice were measured before MCAO procedure, during MCAO procedure and 5 min after MCAO procedure, and there was no difference among three groups (young + PBS + MCAO, aged + PBS or sEVs + MCAO), indicating that MCAO procedure caused equal loss of cerebral blood flow (Figs. S6A–B). The most remarkable difference of polarized phenotype between young and aged stroke mice appears at day 3 after MCAO [13], so we chose this time point for the following experiment. CD16/Iba1 and CD206/Iba1 double-staining was performed to detect M1 and M2 phenotype respectively in both cortex (CTX) and striatum (STR) of the infarct brain tissue as shown in Fig. 4C. The result showed that the percentage of M1-like microglia increased (Fig. 4A–B, 4D and 4F) while the percentage of M2-like microglia decreased (Fig. 4A–B, 4E and 4G) at both CTX and STR in aged stroke mice with PBS treatment compared to that of the young stroke mice with PBS treatment, the iPSC-sEVs treatment significantly reversed this change (Fig. 4A–B and 4D-G). Furthermore, we examined the expression level of inflammatory factors in infarct brain tissue after MCAO by qPCR. The result showed that compared to young stroke mice, M1-like microglia-related pro-inflammatory genes such as CD86, TNF-α and IL-1β were up-regulated in aged stroke mice with PBS treatment, while iPSC-sEVs administration down-regulated their expression (Fig. 4H). Besides, the down-regulated M2-microglia marker (CD206) in aged stroke mice increased after injection of iPSC-sEVs (Fig. 4H). Inflammatory response induced neuronal apoptosis leads to the secondary neuronal damage, which is detrimental to the recovery of brain function [40]. Therefore, we detected whether iPSC-sEVs could protect against neuronal apoptosis in aged ischemic stroke. Tunel and Neun double staining showed that iPSC-sEVs indeed diminished the apoptosis of neuron in ischemic stroke in aged mice (Fig. 4I–J). The above results indicated that iPSC-sEVs could improve the pro-inflammatory status and protect neuron from apoptosis in aged ischemic stroke.

3.5. iPSC-sEVs reduced the infarction volume and improved neurological function in aged stroke mice during the acute and subacute phase

To detect whether alleviating microglia senescence could reduce the brain injuries caused by ischemic stroke in aged mice, we assessed the infarction volume and neurological function. MCAO operation caused a larger infarction volume in aged brain compared to that of young brain as shown by MAP-2 staining, and iPSC-sEVs treatment significantly reduced infarction volume (Fig. 5A–B). Then neurological function was evaluated. The result showed that neurological score (NS) was inferior in aged stroke mice with PBS treatment relative to that of young stroke mice with PBS treatment, while NS decreased in the group with iPSC-sEVs treatment at 3 day after MCAO (Fig. 5C). In consistent with NS, neurological deficiency was worse in aged stroke mice with PBS treatment compared to young stroke mice and sEVs improved neurological function as early as 3 day after MCAO (Fig. 5D–H). The time mice spent in contacting (Fig. 5D–E) and removing (Fig. 5D and F) the sticker in adhesive test was significantly reduced and the time mice stayed at rotarod (Fig. 5H) was prolonged. Additionally, in the cylinder test, iPSC-sEVs decreased the asymmetric rate increased in Aged + PBS group from 3 day to 7 day poststroke (Fig. 5G). Taken together, these results demonstrated that iPSC-sEVs exerted significant protective function of brain and improved neurological function deficits in aged stroke mice.

3.6. iPSC-sEVs mitigated elevated inflammation of senescent microglia and reduced neuron cell death via increasing the rictor and p-AKT (s473)

Next, we examined the effect of iPSC-sEVs on senescent microglia under oxygen and glucose deprivation condition (OGD), a model imitates ischemic stroke in vitro [21]. Three groups were exposed to OGD condition (Control + PBS + OGD group; D-gal + PBS + OGD group; D-gal + sEVs + OGD group). After OGD treatment, the percentage of $CD86^+$ cells (Fig. 6A and C) was higher but the percentage of $CD206^+$ cells was lower (Fig. 6B and D) in D-gal + PBS + OGD group compared to control + PBS + OGD group. Incubation with iPSC-sEVs downregulated the percentage of $CD86^+$ cells (Fig. 6A and C), while upregulated the percentage of $CD206^+$ cells (Fig. 6B and D) in D-gal + sEVs + OGD group compared with that of the D-gal + PBS + OGD group. Moreover, qPCR results showed that treatment with iPSC-sEVs reversed the increase of M1-like microglia related genes (CD86, IL-1β, TNF-α) and the decrease of M2-like microglia related genes (CD206, TGF-β, IL-10) in senescent microglia cells subjected to OGD treatment (Fig. 6E). Therefore, iPSC-sEVs could shift senescent microglia from M1 to M2 after OGD. By using a transwell co-culture system (Fig. 6F), we further showed that the percentage of apoptotic neuron cells increased when co-cultured with senescent microglia cells (D-gal + PBS group) compared to that when co-cultured with young microglia cells (Control + PBS group), while co-culture with sEVs treated senescent microglia (D-gal + sEVs group)

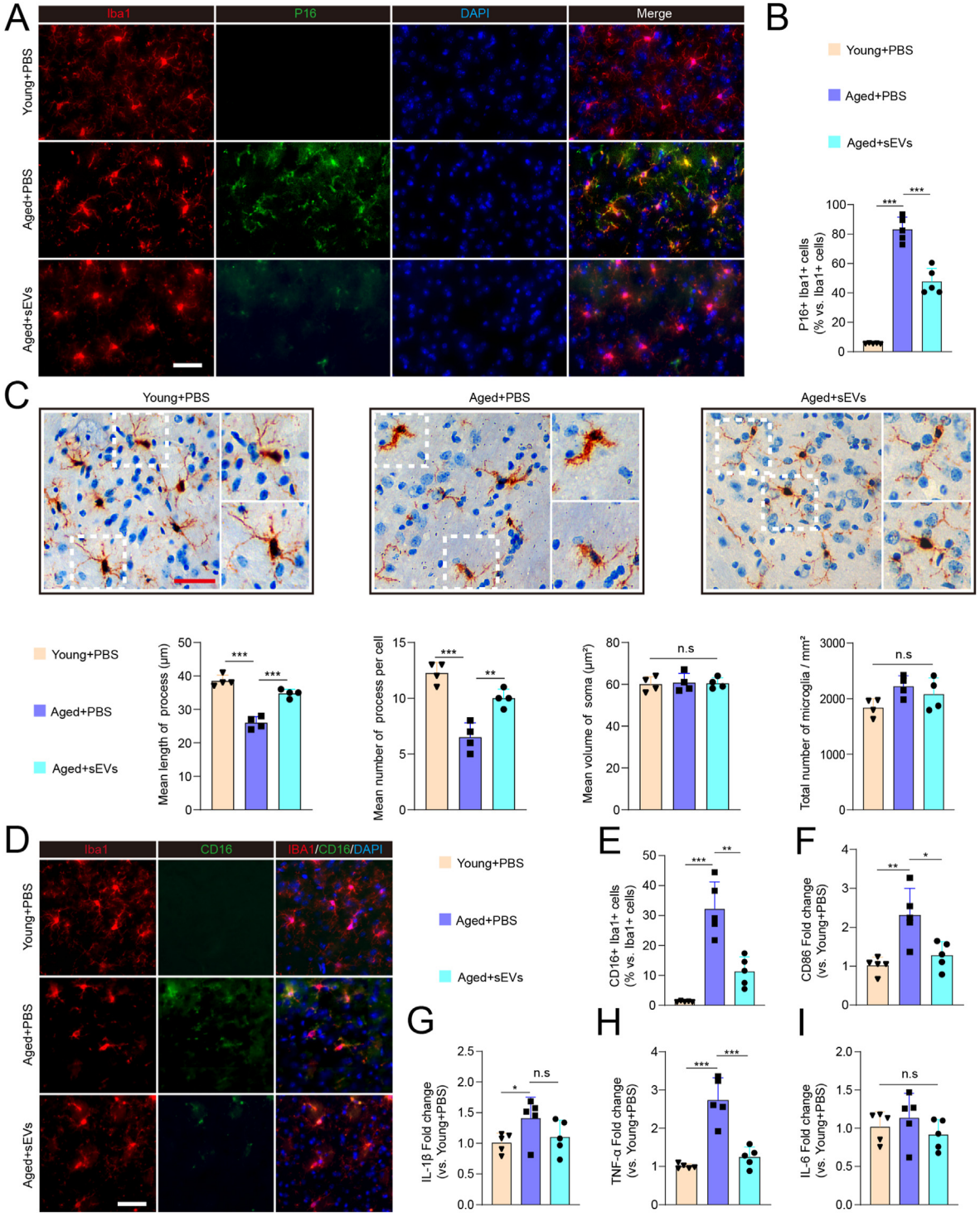

Fig. 3. iPSC-sEVs alleviated microglia senescence and pro-inflammation activation in aged normal brain. (A) Represent fluorescent images of Iba1 (Red)/P16 (Green)/DAPI (Blue) in the brain. Scale bar: 50 μm. **(B)** Quantification of positive percentage of $P16^{+}$ $Iba1^{+}$ cells relative to total $Iba1^{+}$ cells. n = 5 per group. **(C)** Represent immunohistochemical images, and analysis of number and morphological changes of microglia in young mice treated with PBS, aged mice with PBS treatment and aged with sEVs treatment group. Scale bar: 50 μm. n = 4 per group. **(D)** Represent images of Iba1 (Red)/CD16 (Green)/DAPI (Blue). Scale bar: 50 μm. **(E)** Quantification of positive percentage of CD16/Iba1 relative to total $Iba1^{+}$ cells. n = 5 per group. **(F–I)** Quantification of RNA level of M1-related pro-inflammatory genes including CD86 **(F)**, IL-1β **(G)**, TNF-α **(H)** and IL-6 **(I)** relative to young + PBS group. n = 5 per group. Statistical significance was calculated by one-way ANOVA. *P < 0.05, **P < 0.01, ***P < 0.001, and n. s indicated results had no statistical significance. (For interpretation of the references to color in this figure legend, the reader is referred to the Web version of this article.)

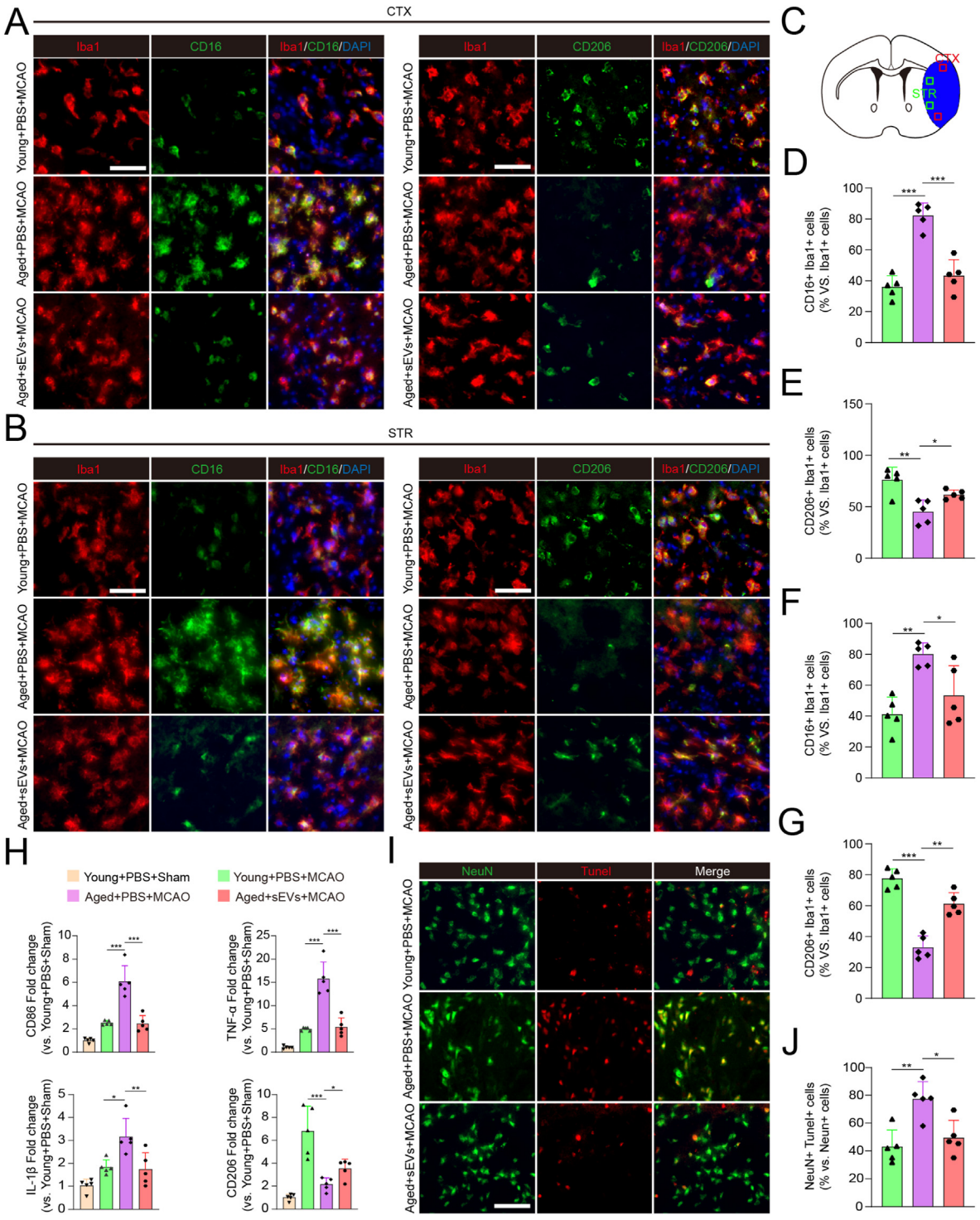

Fig. 4. iPSC-sEVs promoted microglia polarization from M1 to M2 and decreased neuronal apoptosis 3 days after MCAO in aged stroke mice. (A) Represent images of Iba1 (Red)/CD16 (Green)/DAPI (Blue) and Iba1 (Red)/CD206 (Green)/DAPI (Blue) at the infarct border in the CTX. Scale bar: 50 μm. **(B)** Represent images of Iba1 (Red)/CD16 (Green)/DAPI (Blue) and Iba1 (Red)/CD206 (Green)/DAPI (Blue) at the infarct border in the STR. Scale bar: 50 μm. **(C)** Schematic picture of infarct area (Blue) in ischemic stroke. The box (Red) indicated infarct border at CTX and the box (Green) indicated infarct border at STR in ischemic stroke. **(D–E)** Quantification of positive percentage of CD16/Iba1 **(D)** and CD206/Iba1 **(E)** relative to total $Iba1^+$ cells in CTX. n = 5 per group. **(F–G)** Quantification of positive percentage of CD16/Iba1 **(F)** and CD206/Iba1 **(G)** relative to total $IBA1^+$ cells in STR. n = 5 per group. **(H)** Quantification of M1-microglia genes (CD86, IL-1β and TNF-α) and M2-microglia marker (CD206) relative to young + PBS + sham group 3 days after MCAO. n = 5 per group. **(I)** IF staining images of NeuN (Green)/Tunel (Red) 3 days after MCAO. Scale bar: 50 μm. **(J)** Quantification of positive percentage of NeuN/Tunel, which indicated the percentage of apoptotic neuron relative to total $NeuN^+$ cells. Statistical significance was calculated by one-way ANOVA. n = 5 per group. *P < 0.05, **P < 0.01, ***P < 0.001. (For interpretation of the references to color in this figure legend, the reader is referred to the Web version of this article.)

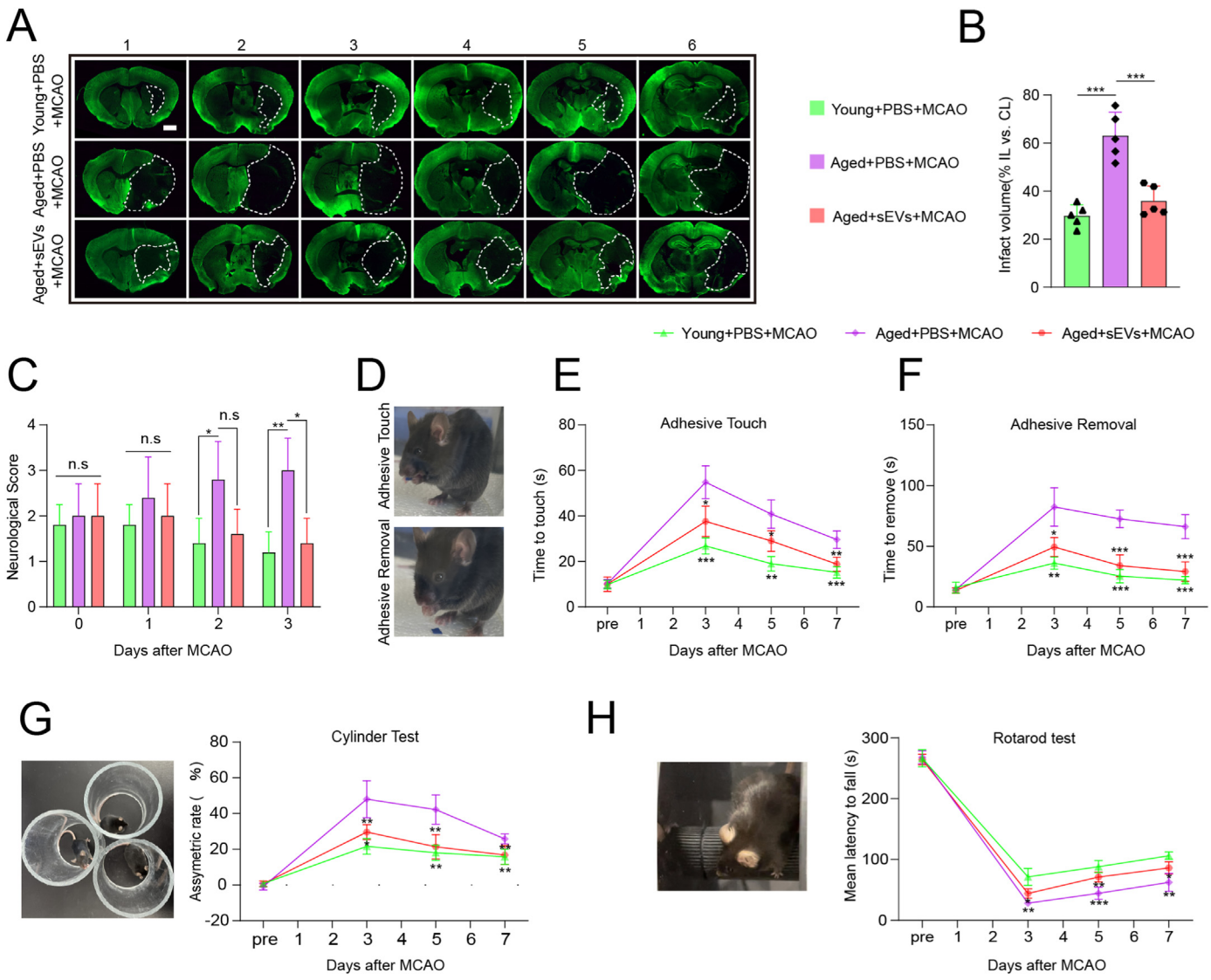

Fig. 5. iPSC-sEVs reduced infarct volume and improved neurological deficits after ischemic stroke in aged mice. (A) IF staining images of MAP-2 (a marker of mature neuron) 3 days after MCAO. The white dashed lines outline the infarct area. Scale bar: 1 mm. **(B)** Quantification of the infarct volume relative to separate contralateral hemisphere. n = 5 per group. **(C)** Quantification of the neurological score (NS) from 0 to 3 days after MCAO. n = 5 per group. **(D–H)** Analysis of behavior tests including adhesive test **(D–F)**, cylinder test **(G)** and Rotarod test **(H)** from before to 7 days after MCAO. n = 5 per group. Statistical significance of **(B)** was calculated by one-way ANOVA. Statistical significance of **(C, E, F, G** and **H)** was calculated by two-way repeated ANOVA. *P < 0.05, **P < 0.01, ***P < 0.001, and n. s indicated results had no statistical significance.

reversed the effect (Fig. 6G and H), indicating that microglia senescence led to the apoptosis of neurons, and relieving the senescence of microglia may protect neurons from cell death after OGD. These results are consistent with the *in vivo* data that iPSC-sEVs treatment reduced the apoptosis of neuron cells in aged stroke mice. Previous study reported that loss of Rictor and downstream p-AKT (s473) led to pro-inflammatory activation of senescent microglia [41]. Here we showed that Rictor and p-AKT (s473) both decreased in D-gal + PBS + OGD group compared to Control + PBS + OGD group (Fig. 6I–K), treatment with iPSC-sEVs reversed the loss of Rictor and p-AKT (s473) (Fig. 6I–K). Next, we used Rictor inhibitor (PP242) [42] to further verify whether iPSC-sEVs-induced modulation of inflammatory response in senescent microglia was related to the activation of Rictor and p-AKT pathway. The addition of inhibitor abolished the iPSC-sEVs-afforded phosphorylation of AKT (Fig. 6L). Moreover, PP242 reversed the effort of iPSC-sEV on alleviation of inflammation as shown by the increased expression of CD86, IL-1β, TNF-α and decreased expression of CD206, TGF-β, IL-10 (Fig. 6M). Besides, pretreatment with iPSC-sEVs also increased the Rictor and p-AKT (S473) in senescent microglia of aged stroke mice, which were both significantly decreased compared to that of young stroke mice (Figs. S7A–C). The above results suggested that iPSC-sEVs could exert significant function on microglia both *in vivo* and in vitro, and the effect of iPSC-sEVs on senescent microglia was at least partially related to the regulation of the expression of Rictor and p-AKT.

iPSC-sEVs regulated inflammatory response of senescent microglia partially via transferring TGF-β1 to upregulate Rictor and p-AKT (s473).

Next, we explored the mechanism how iPSC-EVs reverse the decrease of Rictor in senescent microglia. It is widely accepted that extracellular vesicles exert biological function through delivering active proteins to the recipient cells [43,44]. Thus we looked into the proteomics of iPSC-sEVs we reported previously [45] to determine the active proteins related to the activation of Rictor and AKT in senescent microglia. We found iPSC-sEVs carried TGF-β1, which could upregulate the expression of Rictor and phosphorylation of AKT [46,47]. Western blot results indicated that TGF-β1 were enriched in iPSC and iPSC-sEVs (Fig. 7A). Moreover, we found that the inhibitor of TGF-β1, SB525334 [48],

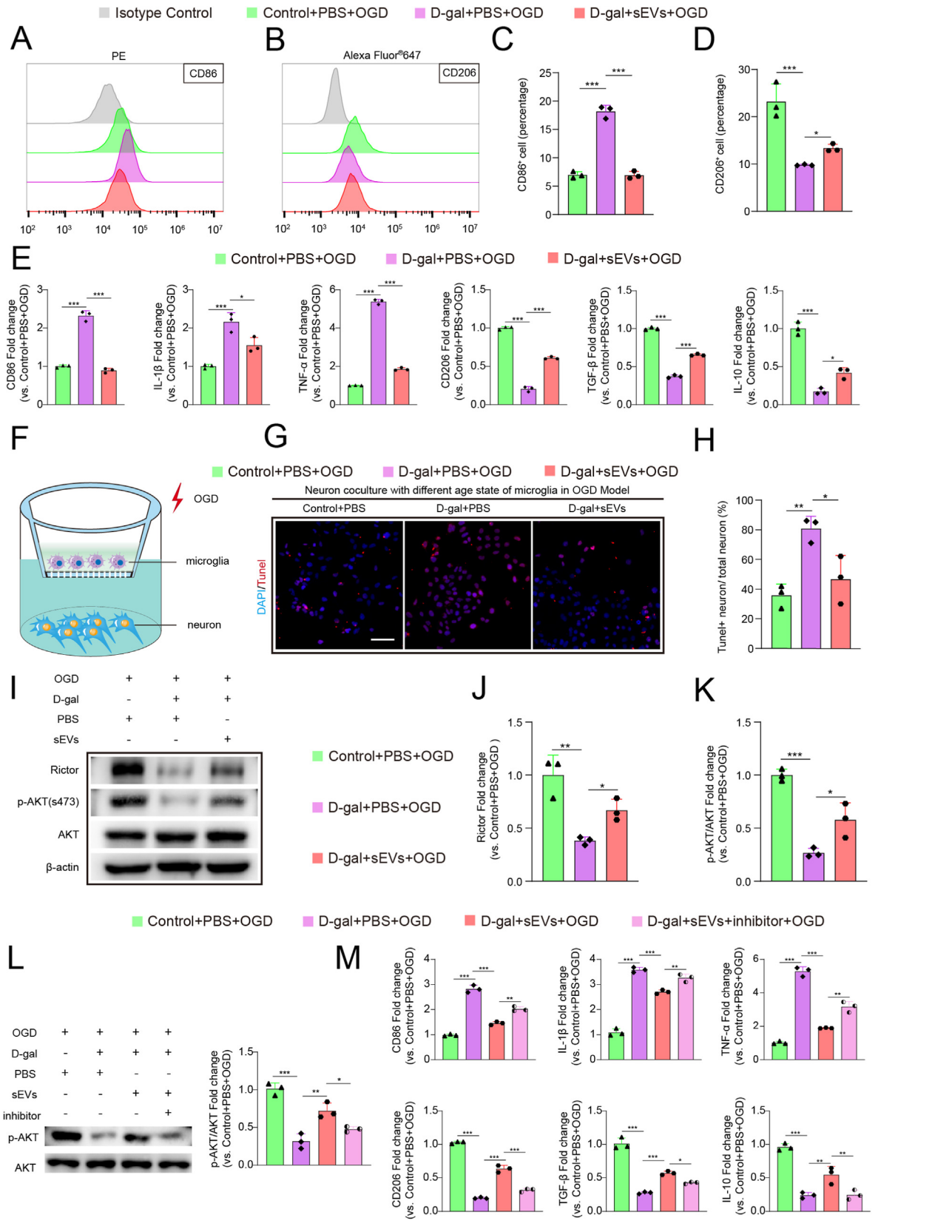

(caption on next page)

Fig. 6. iPSC-sEVs treatment shifted senescent microglia from M1 to M2 and reduced apoptosis of neuron after OGD via increasing the Rictor and p-AKT (s473). **(A–B)** Flow cytometry histogram of $CD86^+$ BV2 cells **(A)** and $CD206^+$ BV2 cells **(B)** after OGD. **(C–D)** Quantification of percentage of $CD86^+$ cells **(C)** and $CD206^+$ cells **(D)** after OGD. n = 3 per group. **(E)** Quantification of M1-microglia genes (CD86, IL-1β and TNF-α) and M2-microglia genes (CD206, TGF-β and IL-10) after OGD relative to Control + PBS + OGD group. n = 3 per group. **(F)** Schematic picture of co-culture system. The different age state of microglia were seeded in upper small chamber and neuron cell line-Sh-sy5y cells were cultured in under hole plate. Then the co-culture system was performed OGD stimulation. **(G)** IF images of apoptotic neuron ($Tunel^+$) in co-cultured transwell respectively with young microglia, senescent microglia and rejuvenated senescent microglia after OGD stimulation. Scale bar: 100 μm. **(H)** Quantification of percentage of apoptotic neuron ($Tunel^+$) related to total neuron in co-culture transwell after OGD. **(I)** Represent western blot bands of Rictor, p-AKT (s473), AKT and β-actin. **(J–K)** Quantification of protein expression of Rictor **(J)** and p-AKT (s473) **(K)**. n = 3 per group. **(L)** Represent western blot bands of p-AKT (s473), AKT and quantification of p-AKT/total AKT. n = 3 per group. **(M)** Quantification of M1-microglia genes (CD86, IL-1β and TNF-α) and M2-microglia genes (CD206, TGF-β and IL-10) after OGD relative to Control + PBS + OGD group. n = 3 per group. Statistical significance was calculated by one-way ANOVA. *P < 0.05, **P < 0.01, ***P < 0.001.

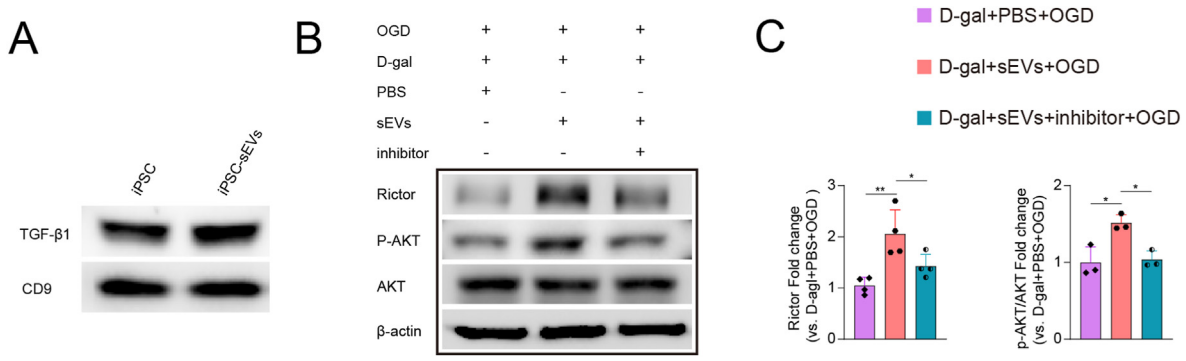

Fig. 7. iPSC-sEVs increased Rictor and p-AKT in senescent microglia through delivering TGF-β1. **(A)** Represent western blot bands of TGF-β1. **(B)** Represent western blot bands of Rictor, p-AKT (s473), AKT and β-actin. **(C)** Quantification of protein expression of Rictor and p-AKT. n = 3 or 4 per group. Statistical significance was calculated by one-way ANOVA. *P < 0.05, **P < 0.01.

blocked the iPSC-sEVs-induced upregulated expression of Rictor and p-AKT (Fig. 7B–C). Taken together, these results demonstrated that iPSC-sEVs reversed the loss of Rictor and p-AKT in senescent microglia to mitigate aggravated inflammation, which was partially related to the delivery of TGF-β1 (Fig. 8).

4. Discussion

Intense inflammation response exaggerates permeability of blood brain barrier [49], the degree of cerebral ischemia-reperfusion (I/R) injury [50] and the neurological deficit after stroke [51]. Microglia, as the innate immune cell in the CNS, can constantly monitor the micro-environment in the "resting" state to maintain homeostasis [32]. When ischemic stroke occurs, microglia are the first cells to respond to the signal of injury and are activated to adapter different polarized phenotypes including classically activated M1 phenotype as well as alternatively activated M2 phenotype [33]. M1 microglia showed adverse effects on the recovery of stroke due to release of pro-inflammatory mediators, such as inducible nitric oxide synthase (iNOS), reactive oxygen species (ROS) and TNF-α; M2 phenotype exert neuroprotective function and promote the survival of neuron by secreting anti-inflammatory mediators, such as brain-derived neurotrophic factor (BDNF), IL-10 and arginase-1 (Arg-1) [33]. Previous studies have proved that promoting microglia to polarize from pro-inflammation type to anti-inflammation type improves outcome of ischemic stroke in young animals [27,52–54]. However, the elder population is vulnerable to ischemic stroke. Recent researches indicate that microglia in aged mice display senescent phenotype [10] and tend to be activated toward to pro-inflammatory phenotype, which causes the worsen outcome in aged stroke mice compared to young stroke mice [13]. Therefore, therapies for the aged population need more attention. In this study, we showed for the first time iPSC-sEVs alleviated microglia senescence both in vitro and *in vivo*, therefore promoted microglia to shift from pro-inflammatory phenotype to anti-inflammatory phenotype in aged stroke mice and improved the outcome of ischemic stroke in aged mice. Mechanism studies showed that iPSC-sEVs could deliver TGF-β1 to promote the expression of Rictor and phosphorylation of AKT, which was involved in the pro-inflammatory phenotype of senescent microglia. Our work demonstrated iPSC-sEVs may be a promising therapy for aged stroke population.

Senescent microglia lose the quiescent state and become activated with a imbalance between pro-inflammatory phenotype and anti-inflammatory phenotype [55]. We found that D-gal induced microglia and microglia in 18-month aged mice both displayed senescent phenotype. Senescent microglia became pro-inflammatory phenotype with the increasing expression of M1 marker (CD16, CD86) and release of TNF-α and IL-1β. When stimulated by ischemic injury, senescent microglia showed more pro-inflammatory phenotype while less anti-inflammatory phenotype, which was accompanied by greater infarct volume and worse neurological function in the aged stroke mice compared to young stroke mice. Importantly, direct evidence that senescent microglia increased death of neuron was firstly shown in this paper, which might due to the increased inflammatory factors released by senescent microglia. Since imbalance of inflammatory response caused by senescent microglia deteriorated outcome of aged ischemic stroke, alleviating microglia senescent would be a novelty idea to treat aged ischemic stroke.

Recent researches indicated that stem cells and stem cells derived sEVs (stem cells-sEVs) possess anti-aging ability and exerted protective function in multiple ageing-associated disorder [15,16,18,56]. iPSCs, generated via genetic reprogramming of adult somatic cells [57], have the following advantages: iPSCs can be expanded unlimited [18] and can be generated from patient-specific somatic cells [19,20], therefore avoiding of immunological rejection. Besides, sEVs possess the similar function to their parent cells and the advantages including low immunogenicity [58] as well as low risk of vascular embolization [59] compared to cells translation. Therefore, iPSCs-sEVs might be an excellent choice for ageing-related diseases, especially for anti-brain aging due to their characteristic of easily crossing the BBB [60]. In this study, we demonstrated that iPSC-sEVs alleviated microglia senescence *in vivo* and in vitro as shown by the decreased expression of ageing-related proteins

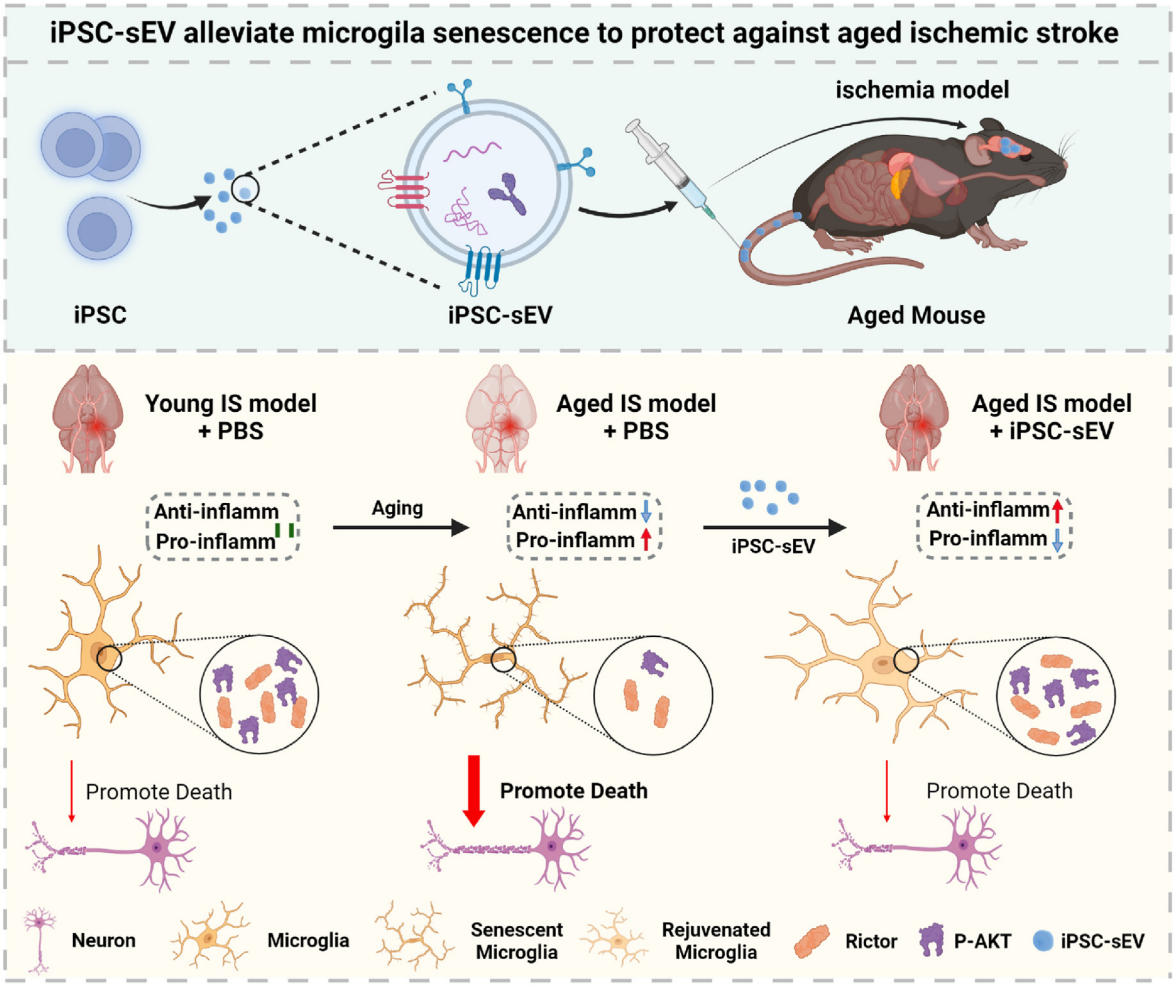

Fig. 8. Schematic illustration of the therapeutic function of iPSC-sEVs on aged ischemic stroke through alleviating microglia senescence. Senescent microglia in aged brain became prodominant pro-inflammatory activation compared to microglia in young brain, which increased the death of neuron and aggravated injury in aged ischemic stroke compared to young ischemic stroke. Treatment with iPSC-sEVs alleviated microglia senescence and promoted microglia activation from pro-inflammatory to anti-inflammatory phenotype via reversing the loss of Rictor and p-AKT (s473) in senescent microglia, which reduced the death of neuron and improved the outcome of aged ischemic stroke.

and the activity of SA-β-Gal, which promoted microglia polarization from pro-inflammatory phenotype to anti-inflammatory phenotype and improved the outcome in aged ischemic stroke. It was worth pondering that whether the anti-aging ability of iPSC-sEVs was specific. Therefore, we explored the anti-aging ability of fibroblast-sEVs and iMSC-sEVs on senescent microglia. As shown in Fig. S3, the results indicated that fibroblast-sEVs had little effect on the senescence of microglia. While iMSC-sEVs indeed alleviate senescence of microglia but the effect was inferior compared to iPSC-sEVs, which demonstrated that treatment with iPSC-sEVs was more suitable relative to MSC-sEVs in the matter of anti-aging ability on senescent microglia. Besides, there were some reports about anti-senescence ability of MSC-sEVs, such as anti-senescence of cardiomyocyte [61] and renal epithelial cells [62], which suggest that MSC-sEVs could be a choice for rejuvenating senescent cells. Rictor, as the key component of mammalian target of rapamycin complex2 (mTORC2) [63,64], can regulate cell senescence by phosphorylating AKT. Recent studies indicate that activation of Rictor/p-AKT signaling pathway prevents the senescence both in endothelial cells [65] and circulating angiogenic cells [66]. In this paper, we found that Rictor and p-AKT (s473) were both decreased in D-gal induced senescent microglia, which was consistent with previous study [41]; Treatment with iPSC-sEVs reversed the loss of Rictor and p-AKT (s473) after OGD, while the inhibitor of Rictor abolished the effect of iPSC-sEVs on alleviating inflammation, which indicated that the function of iPSC-sEVs on regulating senescent phenotype of microglia was at least partially related to the increase of Rictor and phosphorylation of AKT. Furthermore, we looked into our previous proteomics research, and found TGF-β1 was enriched in iPSC-sEVs to upregulate Rictor. Blocking the TGF-β1 could abolished iPSC-sEVs-induced expression of Rictor and p-AKT. Taken together, iPSC-sEVs alleviated microglia senescence, attenuated pro-inflammatory activation of microglia in sham condition and shifted microglia from pro-inflammatory phenotype to anti-inflammatory phenotype, at least, via delivering TGF-β1 to reverse the loss of Rictor and p-AKT (s473) in senescent microglia, which protected neuron from death and improved the aged ichemic stroke (Fig. 7). However, there were some limitations in our research. The fluorescence intensity in the brain was not intense after the single administration of PKH26-labelled sEVs. In our experiments, sEVs were administrated for two months in mice, and we found that iPSC-sEVs indeed rejuvenated senescent phenotype of microglia in aged brain and improved outcome of aged ischemic stroke. Meanwhile, the mechanism of sEVs on regulating microglia we explored in vitro was verified in aged mice. The above results indicated that sEVs could cross BBB and target microglia directly to exert therapeutic function on aged ischemic stroke. Increase of the brain

targeting ability of sEVs [32] may further enhance therapeutic effect against CNS disease. Meanwhile, we cannot exclude the possibility that the effects of iPSC-sEVs on microglia may also through affecting other organs. Additionally, our previous work showed that ESC-sEVs could modulate the function of regulatory T cells (Treg) [26], and iPSC-sEVs might have an indirect impact on microglia through regulating Treg. Besides, sEVs secreted by liver in plasma could entry to brain via the choroid plexus, which could mediate the communication between brain and periphery according to a recent report [67]. Therefore, the effect of sEVs on peripheral organs might regulate the function of microglia, which need to be further explored in the future. It is reported that neuroinflammation caused by senescent microglia contribute to the development of neurodegenerative disease [36], our study might offer a new therapy for ageing-associated Alzheimer's disease and Parkinson's disease.

5. Conclusion

This study demonstrated that iPSCs-sEVs improved inflammatory microenvironment and facilitated the shift of microglia polarization from pro-inflammatory phenotype to anti-inflammatory phenotype through alleviating microglia senescence, therefore protected neuron from death and improved outcome of aged ischemic stroke. As the anti-ageing nanovesicles, iPSCs-sEVs provide a novelty therapeutic strategy for aged ischemic stroke and other ageing-associated neurodegenerative disease.

Author contributions

Xinyu Niu: Conceptualization, Methodology, Formal analysis, Investigation, Data curation, Writing – original draft, Project administration. **Yuguo Xia**: Conceptualization, Methodology, Formal analysis, Investigation, Data curation, Writing – original draft, Project administration, Funding acquisition. **Lei Luo**: Resources, Project administration. **Yu Chen**: Resources, Data curation, **Ji Yuan**: Resources, Investigation. **Juntao Zhang**: Methodology, Resources, Validation, Formal analysis. **Xianyou Zheng**: Validation, Data curation, Funding acquisition. **Qing Li**: Validation, Data curation, Writing – review & editing, Project administration, Supervision. **Yang Wang**: Validation, Data curation, Writing – review & editing, Supervision, Funding acquisition. **Zhifeng Deng**: Validation, Data curation, Writing – review & editing, Supervision, Funding acquisition.

Declaration of competing interest

The authors declare that they have no known competing financial interests or personal relationships that could have appeared to influence the work reported in this paper.

Data availability

The data that has been used is confidential.

Acknowledgement

This study was kindly funded by the National Natural Science Foundation of China (Grant No. 82071371, 82172421 and 82201543), National Postdoctoral Program for Innovative Talent (Grant No. BX20220356), and National Postdoctoral Program (Grant No. 2022M723562).

Appendix A. Supplementary data

Supplementary data to this article can be found online at https://doi.org/10.1016/j.mtbio.2023.100600.

References

[1] Valery L. Feigin, Global, regionall, and national burden of neurological disorders, 1990-2016: a systematic analysis for the Global Burden of Disease Study 2016, Lancet Neurol. 18 (5) (2019) 459–480.
[2] V. Saini, L. Guada, D.R. Yavagal, Global epidemiology of stroke and access to acute ischemic stroke interventions, Neurology 97 (20 Suppl 2) (2021) S6–s16.
[3] K. Shi, et al., Global brain inflammation in stroke, Lancet Neurol. 18 (11) (2019) 1058–1066.
[4] H. Worthmann, et al., The temporal profile of inflammatory markers and mediators in blood after acute ischemic stroke differs depending on stroke outcome, Cerebrovasc. Dis. 30 (1) (2010) 85–92.
[5] K.L. Lambertsen, B. Finsen, B.H. Clausen, Post-stroke inflammation-target or tool for therapy? Acta Neuropathol. 137 (5) (2019) 693–714.
[6] D. Wang, et al., FGF21 alleviates neuroinflammation following ischemic stroke by modulating the temporal and spatial dynamics of microglia/macrophages, J. Neuroinflammation 17 (1) (2020) 257.
[7] R. Kang, et al., The dual role of microglia in blood-brain barrier dysfunction after stroke, Curr. Neuropharmacol. 18 (12) (2020) 1237–1249.
[8] M. Kanazawa, et al., Microglia and monocytes/macrophages polarization reveal novel therapeutic mechanism against stroke, Int. J. Mol. Sci. 18 (10) (2017).
[9] Q. Xia, et al., TRIM45 causes neuronal damage by aggravating microglia-mediated neuroinflammation upon cerebral ischemia and reperfusion injury, Exp. Mol. Med. 54 (2) (2022) 180–193.
[10] M. Ogrodnik, et al., Whole-body senescent cell clearance alleviates age-related brain inflammation and cognitive impairment in mice, Aging Cell 20 (2) (2021), e13296.
[11] W.J. Streit, et al., Dystrophic microglia in the aging human brain, Glia 45 (2) (2004) 208–212.
[12] M.R. Stojiljkovic, et al., Phenotypic and functional differences between senescent and aged murine microglia, Neurobiol. Aging 74 (2019) 56–69.
[13] J. Suenaga, et al., White matter injury and microglia/macrophage polarization are strongly linked with age-related long-term deficits in neurological function after stroke, Exp. Neurol. 272 (2015) 109–119.
[14] S.C. Zhao, et al., Age-related differences in interferon regulatory factor-4 and -5 signaling in ischemic brains of mice, Acta Pharmacol. Sin. 38 (11) (2017) 1425–1434.
[15] L. Gong, et al., Human ESC-sEVs alleviate age-related bone loss by rejuvenating senescent bone marrow-derived mesenchymal stem cells, J. Extracell. Vesicles 9 (1) (2020), 1800971.
[16] G. Hu, et al., ESC-sEVs rejuvenate aging hippocampal NSCs by transferring SMADs to regulate the MYT1-egln3-sirt1 Axis, Mol. Ther. 29 (1) (2021) 103–120.
[17] G. Hu, et al., ESC-sEVs rejuvenate senescent hippocampal NSCs by activating lysosomes to improve cognitive dysfunction in vascular dementia, Adv. Sci. 7 (10) (2020), 1903330.
[18] S. Liu, et al., Highly purified human extracellular vesicles produced by stem cells alleviate aging cellular phenotypes of senescent human cells, Stem Cell. 37 (6) (2019) 779–790.
[19] F.V. Okur, et al., Osteopetrotic induced pluripotent stem cells derived from patients with different disease-associated mutations by non-integrating reprogramming methods, Stem Cell Res. Ther. 10 (1) (2019) 211.
[20] G.W. Hu, et al., Exosomes secreted by human-induced pluripotent stem cell-derived mesenchymal stem cells attenuate limb ischemia by promoting angiogenesis in mice, Stem Cell Res. Ther. 6 (1) (2015) 10.
[21] Y. Xia, et al., Small extracellular vesicles secreted by human iPSC-derived MSC enhance angiogenesis through inhibiting STAT3-dependent autophagy in ischemic stroke, Stem Cell Res. Ther. 11 (1) (2020) 313.
[22] J. Liao, et al., Enhanced efficiency of generating induced pluripotent stem (iPS) cells from human somatic cells by a combination of six transcription factors, Cell Res. 18 (5) (2008) 600–603.
[23] X. Liu, et al., Integration of stem cell-derived exosomes with in situ hydrogel glue as a promising tissue patch for articular cartilage regeneration, Nanoscale 9 (13) (2017) 4430–4438.
[24] C. Théry, et al., Minimal information for studies of extracellular vesicles 2018 (MISEV2018): a position statement of the International Society for Extracellular Vesicles and update of the MISEV2014 guidelines, J. Extracell. Vesicles 7 (1) (2018), 1535750.
[25] Y. Tian, et al., Protein profiling and sizing of extracellular vesicles from colorectal cancer patients via flow cytometry, ACS Nano 12 (1) (2018) 671–680.
[26] Y. Xia, et al., Embryonic stem cell derived small extracellular vesicles modulate regulatory T cells to protect against ischemic stroke, ACS Nano 15 (4) (2021) 7370–7385.
[27] L. Feng, et al., Neutrophil-like cell-membrane-coated nanozyme therapy for ischemic brain damage and long-term neurological functional recovery, ACS Nano 15 (2) (2021) 2263–2280.
[28] Y. Yang, et al., ST2/IL-33-Dependent microglial response limits acute ischemic brain injury, J. Neurosci. 37 (18) (2017) 4692–4704.
[29] B. Chen, et al., Human embryonic stem cell-derived exosomes promote pressure ulcer healing in aged mice by rejuvenating senescent endothelial cells, Stem Cell Res. Ther. 10 (1) (2019) 142.
[30] W. Yu, et al., Rescuing ischemic stroke by biomimetic nanovesicles through accelerated thrombolysis and sequential ischemia-reperfusion protection, Acta Biomater. 140 (2022) 625–640.
[31] Q. Bao, et al., Simultaneous blood-brain barrier crossing and protection for stroke treatment based on edaravone-loaded ceria nanoparticles, ACS Nano 12 (7) (2018) 6794–6805.

[32] J. Shi, et al., Engineering CXCL12 biomimetic decoy-integrated versatile immunosuppressive nanoparticle for ischemic stroke therapy with management of overactivated brain immune microenvironment, Small Methods 6 (1) (2022) e2101158.
[33] N. Yin, et al., Engineered nanoerythrocytes alleviate central nervous system inflammation by regulating the polarization of inflammatory microglia, Adv. Mater. 34 (27) (2022) e2201322.
[34] P.N.N. Nguyen, et al., miR-524-5p of the primate-specific C19MC miRNA cluster targets TP53IPN1- and EMT-associated genes to regulate cellular reprogramming, Stem Cell Res. Ther. 8 (1) (2017) 214.
[35] R.E. von Leden, et al., Age exacerbates microglial activation, oxidative stress, inflammatory and NOX2 gene expression, and delays functional recovery in a middle-aged rodent model of spinal cord injury, J. Neuroinflammation 14 (1) (2017) 161.
[36] D.M. Angelova, D.R. Brown, Microglia and the aging brain: are senescent microglia the key to neurodegeneration? J. Neurochem. 151 (6) (2019) 676–688.
[37] C.N. Parkhurst, W.B. Gan, Microglia dynamics and function in the CNS, Curr. Opin. Neurobiol. 20 (5) (2010) 595–600.
[38] D. Davalos, et al., ATP mediates rapid microglial response to local brain injury in vivo, Nat. Neurosci. 8 (6) (2005) 752–758.
[39] P. Yuan, et al., TREM2 haplodeficiency in mice and humans impairs the microglia barrier function leading to decreased amyloid compaction and severe axonal dystrophy, Neuron 90 (4) (2016) 724–739.
[40] S.C. Zhao, et al., Regulation of microglial activation in stroke, Acta Pharmacol. Sin. 38 (4) (2017) 445–458.
[41] A. Flowers, et al., Proteomic analysis of aged microglia: shifts in transcription, bioenergetics, and nutrient response, J. Neuroinflammation 14 (1) (2017) 96.
[42] Z. Lu, et al., RICTOR/mTORC2 affects tumorigenesis and therapeutic efficacy of mTOR inhibitors in esophageal squamous cell carcinoma, Acta Pharm. Sin. B 10 (6) (2020) 1004–1019.
[43] R. Kalluri, V.S. LeBleu, The biology, function, and biomedical applications of exosomes, Science (6478) (2020) 367.
[44] R. Isaac, et al., Exosomes as mediators of intercellular crosstalk in metabolism, Cell Metabol. 33 (9) (2021) 1744–1762.
[45] Q. Li, et al., Inducible pluripotent stem cell-derived small extracellular vesicles rejuvenate senescent blood-brain barrier to protect against ischemic stroke in aged mice, ACS Nano 17 (1) (2023) 775–789.
[46] P. Abeyrathna, et al., Calpain-2 activates Akt via TGF-β1-mTORC2 pathway in pulmonary artery smooth muscle cells, Am. J. Physiol. Cell Physiol. 311 (1) (2016) C24–C34.
[47] J. Li, et al., Rictor/mTORC2 signaling mediates TGFβ1-induced fibroblast activation and kidney fibrosis, Kidney Int. 88 (3) (2015) 515–527.
[48] K. Sugimoto, et al., Activated microglia in a rat stroke model express NG2 proteoglycan in peri-infarct tissue through the involvement of TGF-β1, Glia 62 (2) (2014) 185–198.
[49] C. Yang, et al., Neuroinflammatory mechanisms of blood-brain barrier damage in ischemic stroke, Am. J. Physiol. Cell Physiol. 316 (2) (2019) C135–c153.
[50] X. Xu, et al., Annexin A1 protects against cerebral ischemia-reperfusion injury by modulating microglia/macrophage polarization via FPR2/ALX-dependent AMPK-mTOR pathway, J. Neuroinflammation 18 (1) (2021) 119.
[51] M. Liu, et al., Cottonseed oil alleviates ischemic stroke injury by inhibiting the inflammatory activation of microglia and astrocyte, J. Neuroinflammation 17 (1) (2020) 270.
[52] X. Hu, et al., Extracellular vesicles from adipose-derived stem cells promote microglia M2 polarization and neurological recovery in a mouse model of transient middle cerebral artery occlusion, Stem Cell Res. Ther. 13 (1) (2022) 21.
[53] X. Liu, et al., Interleukin-4 is essential for microglia/macrophage M2 polarization and long-term recovery after cerebral ischemia, Stroke 47 (2) (2016) 498–504.
[54] J. Pan, et al., Malibatol A regulates microglia M1/M2 polarization in experimental stroke in a PPARγ-dependent manner, J. Neuroinflammation 12 (2015) 51.
[55] M.Y. Wendimu, S.B. Hooks, Microglia phenotypes in aging and neurodegenerative diseases, Cells 11 (13) (2022).
[56] X. Xiao, et al., Mesenchymal stem cell-derived small extracellular vesicles mitigate oxidative stress-induced senescence in endothelial cells via regulation of miR-146a/Src, Signal Transduct. Targeted Ther. 6 (1) (2021) 354.
[57] K.K. Hirschi, S. Li, K. Roy, Induced pluripotent stem cells for regenerative medicine, Annu. Rev. Biomed. Eng. 16 (2014) 277–294.
[58] E.L.A. S, et al., Extracellular vesicles: biology and emerging therapeutic opportunities, Nat. Rev. Drug Discov. 12 (5) (2013) 347–357.
[59] H. Xin, Y. Li, M. Chopp, Exosomes/miRNAs as mediating cell-based therapy of stroke, Front. Cell. Neurosci. 8 (2014) 377.
[60] R.O. Elliott, M. He, Unlocking the power of exosomes for crossing biological barriers in drug delivery, Pharmaceutics 13 (1) (2021).
[61] H. Zheng, et al., Hemin enhances the cardioprotective effects of mesenchymal stem cell-derived exosomes against infarction via amelioration of cardiomyocyte senescence, J. Nanobiotechnol. 19 (1) (2021) 332.
[62] C.M. Liao, et al., Human MSC-derived exosomes reduce cellular senescence in renal epithelial cells, Int. J. Mol. Sci. 22 (24) (2021).
[63] R.C. Hresko, M. Mueckler, mTOR.RICTOR is the Ser473 kinase for Akt/protein kinase B in 3T3-L1 adipocytes, J. Biol. Chem. 280 (49) (2005) 40406–40416.
[64] J. Brown, et al., Mammalian target of rapamycin complex 2 (mTORC2) negatively regulates Toll-like receptor 4-mediated inflammatory response via FoxO1, J. Biol. Chem. 286 (52) (2011) 44295–44305.
[65] C. Yang, et al., Inhibitory effect of 14,15-EET on endothelial senescence through activation of mTOR complex 2/Akt signaling pathways, Int. J. Biochem. Cell Biol. 50 (2014) 93–100.
[66] X. Guo, et al., mTOR complex 2 activation by reconstituted high-density lipoprotein prevents senescence in circulating angiogenic cells, Arterioscler. Thromb. Vasc. Biol. 31 (6) (2011) 1421–1429.
[67] J.H. Lee, et al., Alzheimer's disease protease-containing plasma extracellular vesicles transfer to the hippocampus via the choroid plexus, EBioMedicine 77 (2022), 103903.